J|A|C|S
ARTICLES
Published on Web 11/24/2004

Design and Characterization of Programmable DNA Nanotubes

Paul W. K. Rothemund,*[,†,‡] Axel Ekani-Nkodo,[§,||] Nick Papadakis,[‡] Ashish Kumar,[§] Deborah Kuchnir Fygenson,[§,||,⊥] and Erik Winfree[†,‡]

Contribution from the Departments of Computer Science and Computation and Neural Systems, California Institute of Technology, Pasadena, California 91125, and the Department of Physics, University of California at Santa Barbara, Santa Barbara, California 93106

Received September 17, 2004; E-mail: pwkr@dna.caltech.edu

Abstract: DNA self-assembly provides a programmable bottom-up approach for the synthesis of complex structures from nanoscale components. Although nanotubes are a fundamental form encountered in tile-based DNA self-assembly, the factors governing tube structure remain poorly understood. Here we report and characterize a new type of nanotube made from DNA double-crossover molecules (DAE-E tiles). Unmodified tubes range from 7 to 20 nm in diameter (4 to 10 tiles in circumference), grow as long as 50 μm with a persistence length of $\sim$4 μm, and can be programmed to display a variety of patterns. A survey of modifications (1) confirms the importance of sticky-end stacking, (2) confirms the identity of the inside and outside faces of the tubes, and (3) identifies features of the tiles that profoundly affect the size and morphology of the tubes. Supported by these results, nanotube structure is explained by a simple model based on the geometry and energetics of B-form DNA.

Introduction

Nucleic acids provide a unique material for constructing molecular devices.[1] They support a diversity of structural[2−4] and functional[5−7] motifs governed by predictable properties of the double helix, such as base pairing and stacking, A- and B-form geometries, and energetics. These properties allow the design of DNA complexes analogous to the abstract tiles of mathematical tilings.[8] Such DNA tiles can be programmed to self-assemble into a variety of two-dimensional (2D) arrays.[9−13] Some early designs of 2D arrays accidentally formed tubes,[14,15] and a reexamination of published atomic force microscopy (AFM) images (e.g., ref 10, Figure 4D,E) suggests that many 2D DNA arrays occasionally form tubes rather than flat sheets.

Self-assembled nanotubes of all types[16−19] show great promise for applications that range from nanofabrication to biophysical studies. DNA nanotubes in particular have been reported as templates for the growth of nanoscale conductors.[20,21] Other potential uses of DNA nanotubes are inspired by analogy with the roles of nanotubes and nanofilaments in living cells: as structural supports for the cytoskeleton (e.g., actin filaments), as tracks for the transport of microscopic cargo (e.g., microtubules conveying vesicles), and as moving parts for cellular motility (e.g., flagella). DNA nanotubes may eventually be engineered to mimic all these functions. For biophysics, DNA nanotubes are attractive because we have greater control over the structure, energetics, and dynamics of the DNA tiles than is had over protein monomers for biological tubes. Thus, the effect of molecular changes on macroscopically observable tube properties such as persistence length may be more systematically studied. Further, the development DNA nanomachines[6,22] may

† Department of Computer Science, California Institute of Technology.
‡ Computation and Neural Systems, California Institute of Technology.
§ Physics Department, University of California, Santa Barbara.
|| Materials Research Laboratory, University of California, Santa Barbara.
⊥ Biomolecular Science and Engineering Program, University of California, Santa Barbara.

(1) Seeman, N. C. *Biochemistry* **2003**, *42*, 7259−7269.
(2) Kallenbach, N. R.; Ma, R.-I.; Seeman, N. C. *Nature* **1983**, *305*, 829−831.
(3) Chen, J.; Seeman, N. C. *Nature* **1991**, *350*, 631−633.
(4) Fu, T.-J.; Seeman, N. C. *Biochemistry* **1993**, *32*, 3211−3220.
(5) Panyutin, I. G.; Hsieh, P. *Proc. Natl. Acad. Sci. U.S.A.* **1994**, *91*, 2021−2025.
(6) Yurke, B.; Turberfield, A. J.; Mills, A. P., Jr.; Simmel, F. C.; Neumann, J. L. *Nature* **2000**, *406*, 605−608.
(7) Johnston, W. K.; Unrau, P. J.; Lawrence, M. S.; Glasner, M. E.; Bartel, D. P. *Science* **2001**, *292*, 1319−1325.
(8) Grünbaum, B.; Shephard, G. C. *Tilings and Patterns*; W. H. Freeman and Company: New York, 1987.
(9) Seeman, N. C. *J. Theor. Biol.* **1982**, *99*(2), 237−247.
(10) Winfree, E.; Liu, F.; Wenzler, L. A.; Seeman, N. C. *Nature* **1998**, *394*, 539−544.
(11) Mao, C.; Sun, W.; Seeman, N. C. *J. Am. Chem. Soc.* **1999**, *121*, 5437−5443.
(12) LaBean, T. H.; Yan, H.; Kopatsch, J.; Liu, F.; Winfree, E.; Reif, J. H.; Seeman, N. C. *J. Am. Chem. Soc.* **2000**, *122*, 1848−1860.
(13) Liu, D.; Wang, M.; Deng, Z.; Walulu, R.; Mao, C. *J. Am. Chem. Soc.* **2004**, *126*, 2324−2325.
(14) Krummenacker, M. Personal communication, 2001.
(15) Turberfield, A. J. Personal communication, 2002.
(16) Ghadiri, M. R.; Granja, J.; Milligan, R.; Mcree, D.; Khazanovich, N. *Nature* **1993**, *366*, 324−327.
(17) Fenniri, H.; Mathivanan, P.; Vidale, K. L.; Sherman, D. M.; Hallenga, K.; Wood, K. V.; Stowell, J. G. *J. Am. Chem. Soc.* **2001**, *123*, 3854−3855.
(18) Valery, C.; Paternostre, M.; Robert, B.; Gulik-Krzywicki, T.; Narayanan, T.; Dedieu, J.; Keller, G.; Torres, M.; Cherif-Cheikh, R.; Calvo, P.; Artzner, F. *Proc. Natl. Acad. Sci. U.S.A.* **2003**, *100*, 10258−10262.
(19) Hill, J. P.; Jin, W.; Kosaka, A.; Fukushima, T.; Ichihara, H.; Shimomura, T.; Ito, K.; Hashizume, T.; Ishii, N.; Aida, T. *Science* **2004**, *304*, 1481−1483.
(20) Yan, H.; Park, S. H.; Finkelstein, G.; Reif, J. H.; LaBean, T. H. *Science* **2003**, *301*, 1882−1884.
(21) Liu, D.; Park, S. H.; Reif, J. H.; Yan, H. *Proc. Natl. Acad. Sci. U.S.A.* **2004**, *101*, 717−722.

10.1021/ja044319l CCC: $27.50

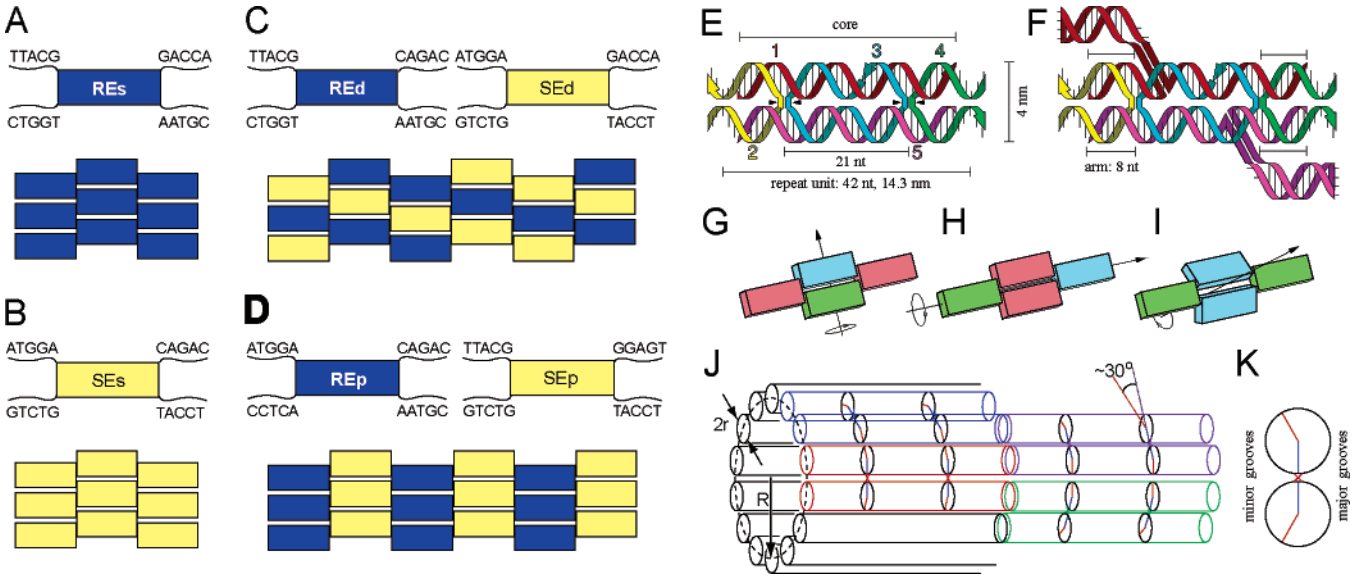

Figure 1. Design and modelling of DNA nanotubes. (A) Top: a single tile REs, based on the core RE, bears 4 sticky ends. Bottom: Complementarity between sticky ends directs the tiles to form a regular lattice. (B) A single tile SEs, based on a difference core SE, and its lattice. (C) Two tiles, REd and SEd, can assemble into a lattice with diagonal stripes; alone each tile could assemble into a linear strip. (D) Another pair of tiles, REp and SEp, cannot assemble independently but together can form a lattice with stripes perpendicular to the long axis of the tiles. (E) Structure of a DAE-E molecule. Each tile is assembled from five single strands: two of 37 nucleotides (nt) (top and bottom, no. 1 and no. 5, red and magenta), two of 26 nt (left and right, no. 2 and no. 4, yellow and green) and one of 42 nt (central, no. 3, blue). Triangles mark two crossover points, separated by two helical turns (21 nt). Arrowheads point from 5′ to 3′. Sticky ends (5 nt) are at the ends of the no. 2 and no. 4 strands. (F) Tile structure with hairpins (8 nt stem, 4 nt loop) on the no. 1 and no. 5 strands between the 14th and 15th nt from their 5′ ends. Molecular models suggest that these hairpins attach underneath the molecule, as depicted here; in a tube they would be on the outside. (G and H) Two in-plane rotational symmetries that, if satisfied by a patch of tiles, encourage molecular strain to balance, resulting in a flat sheet. (I) A rotational symmetry, satisfied by DAE-E molecules, that permits curvature. (J) Heptagonal tube of radius *R*. In each tile, two cylinders of radius r represent the double-helices. Black circles mark crossover points. Blue and orange lines connect the position of phosphate backbones to the center of a helix. The smaller angle between the blue and orange lines defines the minor groove. Tiles from (A), (B), or (D) may form tubes of any number of tiles in circumference; tiles from (C) only tubes of an even number. (K) Cross-section of the red tile from (J) at a crossover point.

allow new kinds of biophysical measurements wherein force-generating DNA machines are used to probe tube structure. Thus, the development of DNA nanotubes as a model system[23] may shed light on principles and phenomena common to many biological nanotubes.

Why 2D DNA arrays sometimes form tubes and how one may design tiles to form tubes reliably, with desired properties, are important open questions. So far, two DNA systems have been reported explicitly as tube-forming. In the first system,[20] the symmetry of the tiles used is cited as consistent with tube formation but the detailed geometry of the tubes and the reasons for their formation remain uncharacterized—it is unknown, for example, which side of a tile is on the outside of these tubes and if it is consistently so. In the second system,[21] tube formation is controlled by disulfide bonds between tiles augmented with thiol moieties; while better understood, this system lacks the flexibility of DNA-only constructions whose formation and geometry can be controlled by other DNA nanomachines.[24,25] Here, we introduce a new DNA-only nanotube motif based on double-crossover (DX) molecules,[4] discovered during investigations of algorithmic self-assembly.[26] Characterization of these tubes confirms our model of tube structure and validates one set of design principles for the reliable formation of DNA tubes. Further, we demonstrate that the tubes are relatively stiff, may be programmably patterned, and may bear chemical modifications directed specificly to their inside or outside.

Design and Modeling

Our DNA nanotubes are based on the programmable assembly of DNA tiles. Conceptually, a DNA tile (Figure 1A) has two parts: (1) a central *core* of DNA, shown as a rectangle, and (2) four single-stranded sticky ends which allow it to bind to other tiles. Here, tiles (Figure 1E) are DX molecules of the DAE-E type[4,27] (nomenclature below). The core is composed of five pseudoknotted strands that form two double helical domains held rigidly by a pair of crossover points. Two different sequence assignments to this structure yield the two different cores, which we call RE and SE, used in the majority of this study. Given an appropriate set of sticky ends, a single core yields a single tile that can self-assemble into a lattice (Figure 1A,B). The use of unique codes for sticky-end sequences allows the interactions between tiles to be programmed. Parts C and D of Figure 1 show how two tiles may be used to create lattices with stripes either diagonal to or perpendicular to the long axis of the tiles. A set of tiles is viewed as a program for the construction of a particular structure. Lowercase letters such as “s”, “d”, or “p” denote a particular choice of sticky ends and are chosen to evoke the pattern generated by the tile set in which they appear: **s**ingle-tile, **d**iagonally striped, or **p**erpendicularly striped lattice.

In this design sticky ends not only specify the connectivity of tiles, they also encourage tiles to form a rectilinear lattice rather than amorphous aggregates. We assume (1) that sticky ends form short segments of B-form helix and (2) that these segments stack collinearly against the helices of the core—as is observed in crystal structures of

(22) Turberfield, A. J.; Mitchell, J. C.; Yurke, B.; Mills, A. P., Jr.; Blakey, M. I.; Simmel, F. C. *Phys. Rev. Lett* **2003**, *90*, 118102.
(23) Ekani-Nkodo, A.; Kumar, A.; Fygenson, D. K. *Phys. Rev. Lett.* **2004**. In Press.
(24) Liu, F.; Sha, R.; Seeman, N. C. *J. Am. Chem. Soc.* **1999**, *121*, 917−922.
(25) Feng, L.; Park, S. H.; Reif, J. H.; Yan, H. *Angew. Chem., Int. Ed.* **2003**, *42*, 4342−4346.
(26) Rothemund, P. W. K.; Papadakis, N.; Winfree, E. *PLoS Biol.* **2004**. In press.
(27) Winfree, E. In *DNA Based Computers*; Lipton, R. J., Baum, E. B., Eds.; DIMACS Workshop, June 10-12, 1996, Vol. 27 of *DIMACS*, pp 199−221; Providence, RI: American Mathematical Society, 1996.

sticky ends.[28] Such a conformation orients the long axes of tiles parallel to each other and guarantees that there exists a well-specified twist between one tile and the next. Thus, an important design principle is the use of stacked helices to avoid ill-defined or floppy junctions.

While stacked sticky ends encourage tiles to form a rectilinear lattice, they do not determine whether the lattice is flat or curved. How, then, are tiles designed to form tubes? First, it is necessary to give the lattice an appropriate symmetry. Some symmetries are incompatible with a curved geometry, for example those in G or H of Figure 1. (Only symmetries of the phosphate backbone, including the location of sticky-end nicks, are considered. This is valid to the extent that tile structure is independent of sequence and nicks that are internal to the core.) In a patch of tiles with one of these symmetries, any molecular strain that could cause curvature may be balanced by a symmetric molecular strain elsewhere. Seen another way, under these symmetries a curved patch of tiles would map to a patch of opposite curvature; both structures cannot be the minimum energy structure, unless multiple minima exist. Thus, one would expect a patch of tiles with such a symmetry to form a flat lattice. Indeed, previously described DAO-E tiles were designed to form patches with symmetries equivalent to those in G and H (Figure 1), and these tiles form flat sheets at least 8 μm in size.[10] By contrast, the DAE-E tiles used here satisfy only one rotational symmetry (Figure 1I), which is compatible with an intrinsically curved geometry for a patch of tiles—a curved sheet of such tiles would map to the same shape under this symmetry. Similar observations concerning symmetry have been made regarding other DNA tubes.[20]

An appropriate symmetry permits curvature but does not ensure it. Tube formation can be encouraged by designing tiles so that their geometry confers a nonzero curvature to a patch of tiles. Here, this is accomplished by the orientation and spacing of the crossover points, as shown by our model of tube structure (Figure 1J). To understand the model, first consider the crossovers within a tile (Figure 1E). The "antiparallel" nature of the crossover[4] forces the minor grooves of the two helices to face the same direction at a crossover point (pointing up in Figure 1E). Further, the distance between intramolecular crossover points (two complete helical turns) forces the minor grooves at the left crossover to face the same direction as the minor grooves at the right crossover. Thus, the DAE-E tile has a *minor groove face* that displays minor grooves at crossovers and a *major groove face* that displays major grooves at crossover.

Next consider the relative positions of the phosphate backbones and refer to the red tile in Figure 1J. The position of *participant backbones* that exchange at the crossovers are marked by blue lines that connect a backbone's position to the center of its helix. *Nonparticipant* backbones do not exchange and are marked by orange lines. Because the two helices are tangent at the crossover point (Figure 1K, cross section at a crossover) the participant backbones define the plane of the tile. The nonparticipant backbones appear on the minor groove face, each at an angle from the plane of the tile equal to the angular extent of the minor groove, $\sim 150° \pm 10°$ in typical B-form DNA.

Finally, consider the relationship of the red tile to one of its neighbors, say the magenta tile. Along the helix connecting the two tiles, the intermolecular distance from the right crossover of the red tile to the left crossover of the magenta (two complete helical turns) forces the orientation of major and minor grooves to be identical at both crossovers. However, the nonparticipant backbone in the red tile is a participant in the crossovers of the magenta tile, and thus defines the plane of the magenta tile. Hence the angle between the planes of the two tiles is the minor groove angle, $\sim 150° \pm 10°$. From this angle we expect tube closure with between 4 and 9 tiles, or 8 to 18 double helices. Further, the direction of curvature predicts that the minor groove faces will be on the inside of the tube.

In general, DX tiles may have crossover spacings different than that of the particular DAE-E molecule used here, and this may either encourage or prevent tube formation. The coarse factors influencing tile structure are the number of crossovers (e.g., **D**ouble), the orientation of the strands through the crossover (e.g., **A**ntiparallel), the number of half-turns between intramolecular crossovers (e.g., **E**ven), and the number of half-turns between intermolecular crossovers (e.g., **E**ven). Hence the tiles used in this study are called 'DAE-E'. Other spacings that satisfy the DAE-E criteria, for example an alternative but still integral number of full turns between crossover points, would also be subject to the preceding geometrical arguments and would be expected to form tubes similar to those in Figure 1J. The four other antiparallel DX types, DAO-E, DAE-O, and DAO-O, have spacings involving an odd number (**O**) of half-turns and have symmetries that should prevent tube formation (Supporting Information Figure 1). How is DAE-E tube structure affected when the distance *D* between intermolecular crossovers is perturbed slightly from an integral number of turns? A naive hypothesis is that tube curvature will change continuously with *D*. A model of the strain energy in a patch of lattice predicts differently: minimum-energy tubes have a curvature (and hence diameter) that is independent of *D* (Supporting Information Figure 2)—although at high strains the tiles may cease to form tubes altogether. We note that all our arguments assume symmetric DX molecules.

Characterization

In this study, we used several variations of the basic tile design (schema and sequences in Supporting Information Figures 3−6; experimental methods in Supporting Information section 1). Our design is modular: generating the different tiles sets in Figure 1A−D only required replacing strands no. 2 and 4 with versions bearing the desired sticky ends. To distinguish between RE- and SE-based tiles via AFM, we replaced strand no. 1 (red) and strand no. 5 (magenta) in SE-based tiles with variants containing hairpins inserted after nucleotide 14 via a three-way junction,[29] Figure 1F. Hairpins at other positions or half-length hairpins were sometimes used. For fluorescence studies, we labeled strands no. 3 or 5 with 5′ fluorescein (FAM). Modifications of tiles are noted in parentheses after the name of a tile. For example, SEs(1,5:h12, 3:FAM) denotes an SEs tile with hairpins 12 nt from the 5′ end of the no. 1 and no. 5 strands and with a 5′ FAM on its no. 3 strand. Although we found that many modifications of the tiles yield tubes with consistent characteristics (tube length, circumference, and persistence length), other modifications significantly disrupt tube formation, a property which we later used to probe determinants of tube structure.

The methods used for all tile variations and tile sets are illustrated by experiments with the REp+SEp tile set. Stoichiometric quantities of all 10 component strands for the REp and SEp tiles were mixed together in TAE buffer containing 12.5 mM Mg^{2+} and annealed ($\sim$1 °C/min) from 95 °C to room temperature. For such annealing schedules, tiles form first at high temperatures (similar DNA tiles have melting temperatures of 55−70 °C[12,26]), and lattices form later at lower temperatures; REp+SEp tiles begin to form filaments at $\sim$35 °C.[23] At room temperature (the temperature at which all subsequent experiments were performed) we observed long filaments by fluorescence microscopy and AFM (Figure 2A,B). The filaments were largely immobilized; they bind strongly to untreated glass or mica. (Divalent cations such as Mg^{2+} presumably condense between phosphates in the DNA backbone and hydroxyl groups on these surfaces.[30,31]) Filaments appear stable in solution—we have imaged 6-month-old samples successfully.

(28) Qiu, H.; Dewan, J. C.; Seeman, N. C. *J. Mol. Biol.* **1997**, *267*, 881−898.
(29) Ouporov, I. V.; Leontis, N. B. *Biophys. J.* **1995**, *68*, 266−274.
(30) Hansma, H. G.; Laney, D. E. *Biophys. J.***1996**, *70*, 1933−1939.

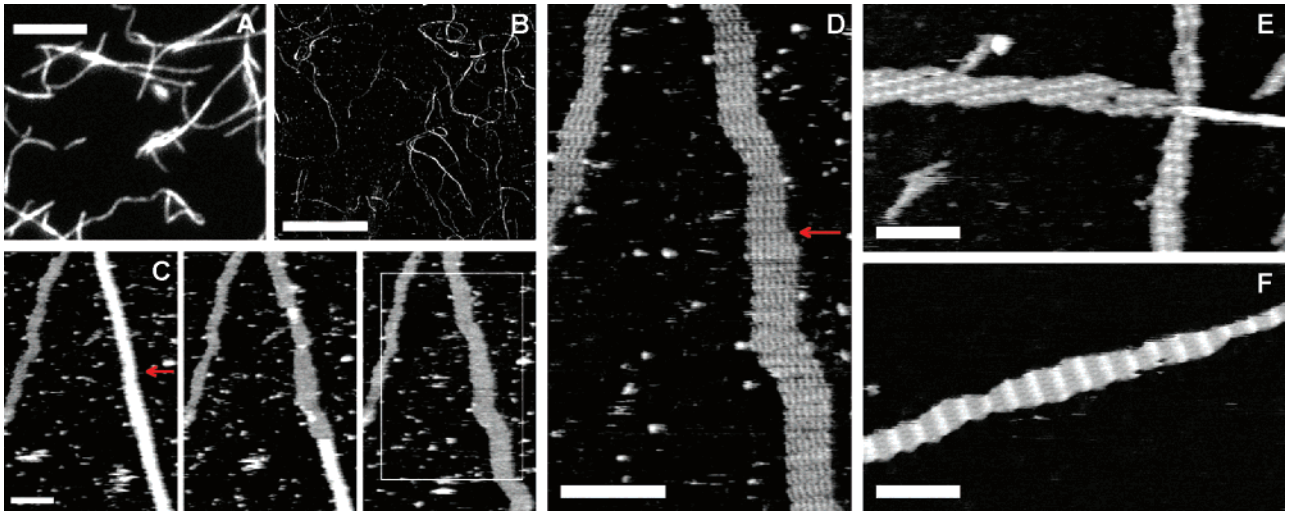

Figure 2. Microscopy of tubes and their programmable ultrastructure. (A−B) Solutions of DNA filaments, visualized by (A) fluorescence microscopy and (B) AFM. The solution in (A) contains REp+SEp(3:FAM) and in (B) contains REp+SEp. Both images were taken at the same tile concentration and magnification. Scale bar, 5 μm. (C) A time series of AFM images indicates that filaments are tubes (REp+SEp). Left: A thick filament (closed tube) runs the length of the image. Heights of closed tubes suggest they are squashed flat. An already-open tube is seen on the left. Center: The tube opens progressively from one end, revealing a one-tile-thick lattice. Bottom: The fully opened tube resembles the lattice on the left. An arrow marks a discrete change in tube width before opening and in the number of tiles after opening, suggesting a defect in the tile lattice. (D) At greater magnification, individual tiles are resolved. (E−F) Open two-tile tubes made from REd+SEd(1,5:h14) (E) and REp+SEp(1,5:h14) (F). Hairpins on SEd or SEp image as diagonal and perpendicular stripes, respectively Scale bars (C−F), 100 nm.

Several basic features of our model were confirmed by high-resolution AFM imaging of REp+SEp filaments. We observed two types of long, narrow filament: thick ones ~3.5−5 nm in height with straight but sometimes streaky edges (right-hand side, Figure 2C) and thin ones ~1.5−2 nm in height with well-defined, jagged but parallel edges (left-hand side, Figure 2C). With successive scans of the same area, thick filaments often turned into thin ones. Such temporal sequences suggest that the thin filaments are closed single-walled tubes which open into sheets. (Unscanned areas often contain closed tubes long after they have all opened in scanned areas, suggesting that tube opening may be hastened by interaction with the AFM tip.) When individual tiles could be resolved, images of such *tube-opening events* provided information about the ultrastructure of tubes. Figure 2D shows that the long axis of the tiles is parallel to the original axis of the closed tube, consistent with Figure 1J. Tiles are spaced ~14 nm along their long axis and ~6 nm in the perpendicular direction with a ~2 nm gap between tiles. Thus, on mica, tiles are not close-packed as shown in Figure 1J. Whether the 6 nm spacing occurs because of a lattice−mica interaction or is representative of tube structure in solution is not known. In either case, the 6 nm spacing raises the question of whether the helix geometry is distorted, for example, by destacked sticky ends. Evidence that sticky ends stack in solution is given in the next section.

Different tile sets behaved as expected. REp or SEp alone did not yield tubes, but reprogramming sticky ends to create either REs or SEs tiles gave tubes similar to those seen in Figure 1C,D, although composed of only a single type of tile. Further changes to the sticky ends and the addition of hairpins resulted in REd and SEd(1,5:h14) tiles that formed tubes with the expected pattern of stripes diagonal to the long axis of the tube (Figure 1E). Similarly, REp and SEp(1,5:h14) tiles formed tubes with a pattern of stripes perpendicular to the long axis of the tubes (Figure 1F). In each of these cases the tile set and the lattice formed varied substantially, with different local arrangements of tiles, patterns of hairpins, symmetries, and molecular structures. Yet, in each case, the tubes that formed were very similar.

Measurements of tube length and circumference were complicated by the dynamic nature of tubes on the mica surface, a problem revealed by imaging the same location for several hours (Supporting Information movie 1). In addition to the deposition and opening of tubes, we observed both the disappearance of tubes and the growth of opened tubes to several times their original width, presumably by the incorporation of tiles from solution. Frequently tubes bound to the mica transiently sometimes leaving behind a small fragment. These, in turn, reoriented or fused with neighboring fragments. Thus, small fragments that appear on the mica do not necessarily represent a population of small lattices or short tubes in solution, precluding accurate measurement of length by AFM.

However, tube circumference can be inferred from tube-opening events. We measured tube width before (w_{before}) and after opening (w_{after}) for 10 tubes of type REp+SEp, REp+SEp-(1,5:h14), or REd+SEd(1,5:h14) for which the number of tiles (n_{after}) could be counted. Consistently, $w_{after} \approx n_{after} \times 6$ nm, and therefore we sometimes use w_{after} to estimate tube circumference in tiles. For long stretches, n_{after} varied by no more than ± 1, suggesting that few tiles were lost during opening. The arrow in Figure 2C,D marks a discrete change in n_{after} that occurred at the same location as a change in w_{before}, suggesting a lattice defect site. Tubes without hairpins are underrepresented in the tube-opening data; in samples based on REs, SEs, or REp+SEp most tubes were already open by the time imaging began, and few or no tube-opening events were observed. (A hairpin-dependent decrease in adhesion appears responsible; Supporting Information section 2.) To obtain more data on the circumference of tubes without hairpins, we applied SEs tubes to mica already wet with a large volume of buffer, and watched

(31) Bustamante, C.; Guthold, M.; Zhu, X.; Yang, G. *J. Biol. Chem.* **1999**, *274*, 16665−16668.

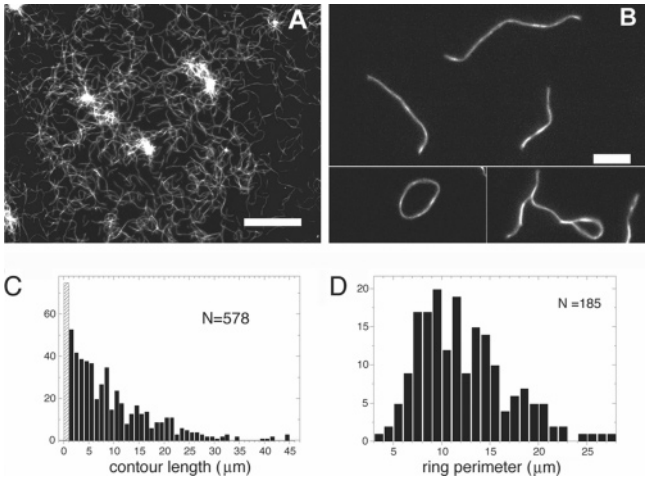

Figure 3. Determination of persistence length. (A) Epifluorescence image of SEs(3:FAM) tubes, imaged at 400 nM tiles, showing aggregation. Tubes diffuse freely in the focal plane. Scale bar, 40 μm. (B) As in (A), but diluted to 40 nM. Intensity variations may indicate regions of different tube width. Occasionally, rings (left) and branched or bundled structures (right) are found. Scale bar, 5 μm. (C) Linear tubes averaging 7 μm in length; ~10% are over 15 μm long, consistent with an exponential distribution. Some tubes reach ~50 μm. (D) Circularized tubes averaging in 12 μm in perimeter with a unimodal distribution. The ring shown is typical; most rings are free of kinks that would indicate local weakness. Since tube length and ring perimeter distributions for REs(3:FAM), SEs(3:FAM), and REp(3:FAM)+SEp(3:FAM) tubes were similar, data in (C) and (D) are aggregate data.

for *tube-falling events*: from one frame to the next, wholly opened tubes appeared on the surface, and w_{after} was measured for five such events. Tube-opening and tube-falling measurements suggest that, for tubes without hairpins, circumference varies at least from 4 to 10 tiles; for tubes with hairpins, circumference varies at least from 3 to 8 tiles. Many w_{after} measurements on subjectively well-isolated tubes are consistent with these ranges. Thus, tube circumference agrees with our model. That the experimental range coincides with the range predicted by uncertainty in minor groove angle seems coincidental; without understanding the flexibility and fluctuations of DNA lattices during nucleation, there is no a priori way to predict the range.

We used fluorescence microscopy to measure length and stiffness in solution. After annealing, we constrained fluorescently labeled tubes to 2D by preparing thin (~3 μm) samples of solution confined between poly(vinylpyrrolidone) (PVP)-coated glass surfaces. The PVP coating was necessary to prevent DNA−surface interactions. At the highest concentration (400 nM tiles) the density of tubes was too high to identify individuals, and clump-like aggregates were common (Figure 3A). Upon 10-fold dilution, single tubes were well dispersed, and occasionally a ring or frayed bundle was seen (Figure 3B). Immediately after annealing, only short tubes were observed. The length distribution matured over the next 16 h (at which point data was taken; Figure 3C) and appeared constant thereafter. Stiffness was inferred from the distribution of ring perimeters (Figure 3D) using a method[32] which assumes that the rate of ring formation for a tube of length L is approximately proportional to the fraction of time that the ends of the tube are co-localized at equilibrium.[33] For short times, during which the length distribution does not significantly change, this rate can be treated as a *ring closure probability* and can be calculated analytically as a function of tube length L and persistence length p. Under these conditions, the distribution of ring perimeters should be the product of the distribution of tube lengths and the ring closure probability. While ring lengths were measured under confinement to an ~3 μm layer, the ring closure probability used is consistent with our assumption that rings formed in the 3D environment of solution. Using the distributions of Figure 3, C and D, we obtained a persistence length of 3.85 ± 0.35 μm (Supporting Information Figure 7).

This persistence length is reasonable, given the model of Figure 1J. We approximate a tube as a ring of rigidly linked rods of known stiffness, given by the persistence of a DNA double helix ($p_{helix} \approx 50$ nm). Under the assumption that Young's modulus is the same for both tubes and helices, the ratio of their persistence lengths is given by ratio of their moments of inertia (derived in Supporting Information section 3):

$$\frac{p_{tube}}{p_{helix}} = \frac{I}{i} = 2N\left[1 + 2\left(\frac{R}{r}\right)^2\right]$$

where i and I are the moments of inertia for the helices and tubes, N is the number of tiles along the circumference, R is the radius of a tube, and r is the radius of a double helix (Figure 1J).

We assume the actual value of R/r lies between that of a close-packed lattice, $2N/\pi$, and that of lattice with the ~6 nm spacing observed by AFM, $3N/\pi$.

Then, the above equation yields an estimates of $p_{tube} \approx 6-12$ μm for $N = 4$ and $p_{tube} \approx 29-63$ μm for $N = 7$. Because the helices are not truly rigid rods and the crossovers and sticky ends are not perfectly rigid links, this simple modeling provides a plausible upper bound for the stiffness of tubes that are defect free and of monodisperse circumference. Given that tubes have lattice defects and variations in diameter, it is not surprising that the measured persistence length should fall somewhat below that predicted for $N = 4$.

Modifications and Structural Perturbations

Our structural model's assignment of the inside and outside of tubes is confirmed by experiments performed to test the hypothesis that large decorations on the inside of the tube would disrupt tube formation. By AFM we examined a series of tubes based on SEs(5:hX) tiles, each bearing a hairpin inserted 3′ of position X on strand no. 5 for $X = 6-31$. (Figure 5A shows the geometric location of these positions; raw AFM data is in Supporting Information Figures 8−10 and is summarized in Supporting Information Figure 17.) Of 10 variants with hairpins predicted to lie on the outside (including $X = 14$, the position used for AFM contrast in the last section) 9 formed normal tubes of circumference from 4 to 10 tiles; one ($X = 24$) gave normal tubes of circumference from 4 to 12. Hairpins at other positions would be located, according to the model, either inside of tubes or between helices. In all these variants normal tube formation was disrupted, but the resulting morphology was quite variable. In the most extreme case, for $X = 29$, no tubes formed (Supporting Information section 4 and Supporting Information Figure 10). To our surprise, many of these samples formed wide but short (0.5−5 μm) *flipped tubes* (Figure 4A) in which the

(32) Sano, M.; Kamino, A.; Okamura, J.; Shinkai, S. *Science* **2001**, *293*, 1299−1301.
(33) Yamakawa, H.; Stockmayer, W. H. *J. Chem. Phys.* **1972**, *57*, 2843−2854.

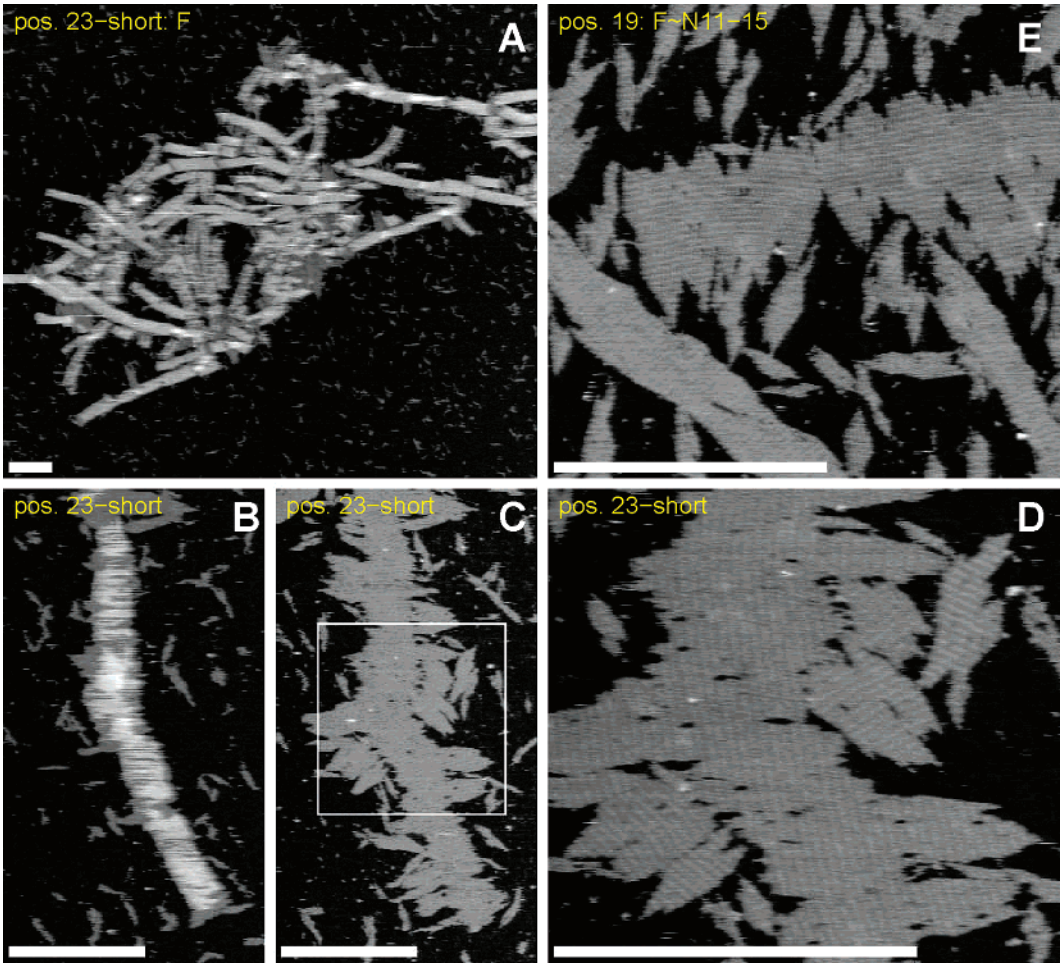

Figure 4. AFM of hairpin insertion experiments. Scale bars, 500 nm. (A) SEs (5:h23-short) flipped tubes; most are closed. For these tubes a shortened hairpin (4-base pairs in the stem) is sufficient to cause all tubes to assume a flipped configuration. (B) A single ~1.5 μm × 175 nm flipped tube from A before (~4 nm in height) and after (C) (~2 nm in height) opening. The width of open tubes is roughly twice that of closed tubes so we infer a tube circumference of 350 nm. (D) An ~500 nm zoom shows that the long axis of the tiles is perpendicular to the long axis of the tube. (E) At some positions inserted hairpins result in a mixture of flipped tubes and normal tubes of large circumference (10−20 tiles), shown here for SEs (5:h19) tiles.

tube axis was perpendicular to the long axis of the tiles (Figure 4D). Opening events for flipped tubes (Figure 4B,C) showed that they can be at least 25 tiles wide (Figure 4D) and thus 115 nm in diameter (Supporting Information movie 2). Some hairpin locations resulted in a mixture of flipped tubes and tubes of the normal orientation (Figure 4E), although the latter tubes tended to be wider and shorter than normal tubes with hairpins on the outside. Hairpins were sometimes visualized between tiles (Supporting Information Figure 11A,B) for positions ($X = 17$, 19) that place hairpins between helices. Except when on the outside, the effects of hairpins are hard to explain. For example, SEs(5:h20) gave exclusively flipped tubes, but the addition of a second hairpin, as in SEs(1,5:h20), gave unusually large normal tubes, 18−28 tiles in circumference (Supporting Information Figure 11C).

As a second test of our model's assignment of inside and outside, we determined which positions were accessible to binding by the protein streptavidin, ~5.4 nm × 5.8 nm × 4.8 nm in size.[34] We presumed that a few streptavidin molecules bound in the mouth of a normal tube would render positions on the inside of a tube inaccessible to further binding. A series of normal tubes were created from tiles, SEs(3:FAM, 5:b*X*), labeled with FAM and bearing a biotin-dT at each of the previously described positions. After annealing, an excess of streptavidin-Cy3 was added and allowed to bind for 10 min before the reaction was quenched with biotin. The ratio of Cy3 and FAM fluorescence on tubes indicated the extent of streptavidin binding. As a control, the same assay was used on SEs(1:h22, 3:FAM, 5:b*X*) flipped tubes which were presumably wide enough (45 nm, Supporting Information Figure 12) to allow streptavidin-Cy3 to diffuse into the interior; thus, binding could occur on both sides of the tiles. Results for normal and flipped tubes are shown in Figure 5B. In normal tubes, green-yellow bands (indicating little or no streptavidin-Cy3 binding) occur for positions where hairpins disrupt normal tube structure (light spheres, Figure 5A), while red-orange bands (indicating accessibility for streptavidin-Cy3 binding) occur for positions where hairpins have little or no effect. The relative orientations of the hairpin and the biotin-dT may play a role in the minor discrepancies in these correlations. In contrast, the flipped tubes were much more accessible to streptavidin-Cy3 binding: only a few bands are green or yellow, and these correspond to putative intramolecular (positions 12, 13, 23) and intermolecular (positions 8, 29) contacts. Biotin at the putative intermolecular

(34) Hendrickson, W. A.; Pahler, A.; Smith, J. L.; Satow, Y.; Merritt, E. A.; Phizackerley, R. P. *Proc. Natl. Acad. Sci. U.S.A.* **1989**, *86*, 2190−2194.
(35) Carter, E. S., II; Tung, C.-S. *CABIOS* **1996**, *12*, 25−30.

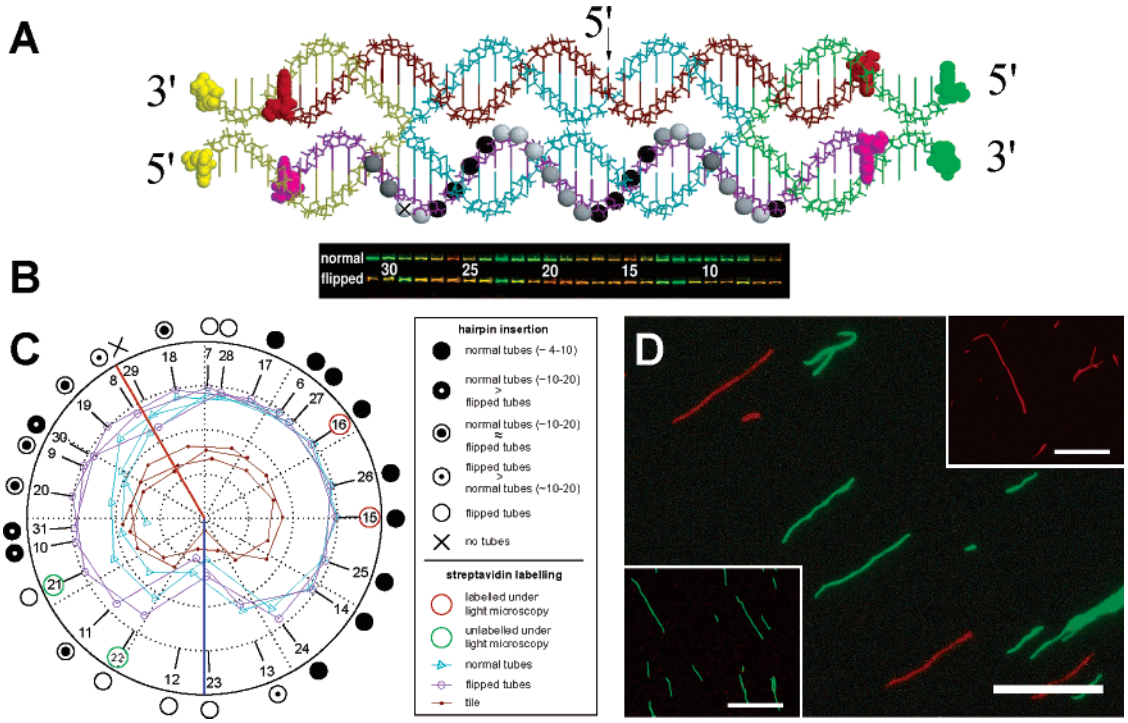

Figure 5. Modifications used to probe tube structure. (A) Molecular model[35] showing the location of modifications. Space-filled bases on the no. 1, 2, 4, and 5 strands indicate where truncations were made to explore the effects of base stacking and on the no. 3 strand where FAM was added. Phosphorus atoms (gray level spheres) show 26 positions (numbered 6−31, right to left, from the 5′ end of the no. 5 strand) at which either hairpins with 8-base pair stems or biotin-dTs were inserted. Five levels of shading show results from the hairpin-insertion experiment. Black spheres indicate that only normal tubes of predominantly small circumference (~4−10 tiles) were observed. Successively lighter spheres indicate mixtures of flipped and normal tubes with successively higher ratios of flipped:normal tubes—the lightest spheres indicate positions at which only flipped tubes are observed. (B) Fluorescent gels showing the results of binding fluorescent streptavidin-Cy3 to biotin-labeled normal tubes SEs(3:FAM, 5:b *X*) and biotin-labeled flipped tubes SEs(1:h22, 3:FAM, 5:b *X*). Gels are aligned for comparison with A. (C) Polar plot summarizing the results of the hairpin insertion and streptavidin binding experiments. Data (arctan[green fluorescence/red fluorescence] or fraction of tiles gel-shifted) are plotted according to a helical twist of 34 °/bp. Circular symbols correspond to the gray level spheres in A. Orange and dark blue lines match Figure 1K. Red and green circles indicate positions tested as in D. (D) Insets showing epifluorescence images of SEs(3:FAM, 5:b22) tubes immobilized and stretched on untreated glass, lower left, and SEs(5:b15) tubes, upper right, after incubation with streptavidin-Cy3. SEs(3:FAM, 5:b21) and SEs(5:b16) gave similar results. At center SEs(3:FAM, 5:b22) and SEs(5:b15) tubes were first mixed and then incubated with streptavidin-Cy3 allowing comparison of the extent of labeling between the two types of tubes. Scale bars, 10 μm.

contact in the middle of the crossover (17−18) may remain accessible to streptavidin binding because of the large lateral gap (~2 nm) observed between tiles when incorporated into tubes. As a further control, binding of streptavidin-Cy3 to tiles that cannot assemble because they have no sticky ends, SEn-(3:FAM, 5:b*X*), was assayed by gel-shift (Supporting Information Figure 13). Tiles labeled uniformly with streptavidin-Cy3 except for positions 12 and 13, the presumed intramolecular contacts. A summary of the hairpin insertion and streptavidin-binding results (Figure 5C) shows that the experimentally determined inside of the tubes correlates well with the angular extent of the minor groove. Supporting Information movie 3 shows a closed-packed model of a heptagonal tube with the hairpin-insertion data labeled as in Figure 5A.

Used with fluorescence microscopy, the streptavidin binding assay shows that the orientation of tube inside and outside is consistent within a population tubes; normal tubes always close in the same direction. Two samples of normal tubes were prepared: the first, SEs(3:FAM, 5:b22), contained a FAM-labeled no. 3 strand and a biotin on the inside; the other, SEs-(5:b15), contained only a biotin on the outside. In the former sample, after adding streptavidin-Cy3 all tubes remain green; in the latter sample, red tubes appear and serve as a positive control (Figure 5D, insets). Only when the two samples were mixed did we see a population of red and green tubes in the same image (Figure 5D, center). Mixed samples were sonicated and rejoined[23] to form hybrid tubes—demonstrating that tubes with multiple chemical characters can be created (Supporting Information Figure 14).

Finally, we explore (1) the importance of stacking and normal B-form helix geometry at the sticky ends and (2) the effect of changing the distance *D* between intermolecular crossovers. To eliminate stacking interactions at specific sticky ends, we used strands in which either the terminal nucleotide of the sticky end or the flanking nucleotide of the sticky end was absent (refer to spaced-filled nucleotides in Figure 5A). All 20 such samples (using RE, SE, or an additional core design VE-00; Supporting Information section 5 and Supporting Information Figures 6, 15, and 17) showed disruption of the tube structure, either mild (unusually wide normal tubes and a high background of small lattice fragments were observed) or more often extreme (flipped tubes were observed, or small lattices were observed, but no tubes could be found). Thus, stacking is necessary for normal tube formation. (Additionally this implies that purified full-length strands are necessary for normal tube formation—an oligonucleotide sample contaminated with a high percentage of (n − 1) truncation products might yield flipped-tube morphology or otherwise affect the properties of the tubes.) We suggest that the 2 nm gap between tiles may be explained by a gentle bending of the normal double helix. Finally, to vary the distance *D*, we changed the lengths of the helical arms connecting the tiles. Assuming that the sticky end between two

tiles adopts an undisturbed B-form geometry, our model of strain energy predicts that this alteration would add strain to a normal tube or prevent tube formation rather than change tube geometry (even though it would change the preferred orientation of a free dimer of tiles). Indeed we found that a one base-pair increase or decrease in D resulted in normal tubes 5−9 tiles in circumference and greater changes in D gave no tubes or lattice at all (Supporting Information section 6 and Supporting Information Figures 3, 6, 16, and 17). This result also suggests sticky-end are stacked: if the nucleotides flanking the sticky end did not stack and were free to rotate, then one might have expected even large changes in D to have no effect on tube formation.

Discussion

To assess the DNA nanotubes' potential as structural material we compared its stiffness to other nanofilaments and nanotubes. The DNA nanotubes' persistence length is 100 times that of double-stranded DNA (∼50 nm),[36] comparable to that of acid-etched carbon nanotubes (800 nm),[32] and F-actin (∼10 μm),[37] but 10 times less than that of pristine single-walled carbon nanotubes (∼50 μm),[38] and 1000 times less than that of microtubules (∼5 mm).[39] More insightful is the question of how efficiently the material in the DNA nanotubes is used, for example how much stiffness is achieved given the linear density λ (mass per unit length in daltons per nm) of the tubes. Depending on whether our measurement of p_{tube} is representative of 4-tile tubes (λ = 15000 daltons/nm) or of 10-tile tubes (λ = 38000 Da/nm), our DNA nanotubes achieve p_{tube}/λ of 0.27 nm^2/Da or 0.11 nm^2/Da, respectively. This is only somewhat less efficient than similar biological filaments: F-actin has λ =16000 Da/nm and so its $p_{\text{filament}}/\lambda$ is ∼0.6 nm^2/Da. Our DNA nanotubes contain defects; more carefully prepared samples are likely to yield higher persistence lengths. Nevertheless, it is remarkable that these purely DNA nanostructures already compete quantitatively with highly evolved proteins for a structural task. This suggests that, similarly, RNA could have played diverse structural roles in an RNA world.

Hairpins were used as AFM contrast markers in the first DX lattices,[10] and their effect on the energetics of lattice formation has been an open question ever since. Our hairpin insertion experiments show that, depending on position, hairpins may have a profound effect on the outcome of a self-assembly reaction. Further, the hairpins effect what seems to be a delicate balance. In many cases, either exclusively normal tubes or flipped tubes form, but in other cases a mixture of morphologies forms. The same types of phenomena are observed for tiles from which 1 or 2 bases have been truncated. Our annealing step was short (∼1 h), and so we do not know if such phenomena are kinetic or thermodynamic. Still, that a broad spectrum of minor changes should exert such profound effects on the morphology of tubes is striking and underlines the need for DNA design tools that explicitly consider molecular geometry and energetic factors.

Flipped tubes were an unexpected effect of perturbing hairpin position, and we have no model for their structure. We do not know if flipped tubes have a consistent inside and outside, or if flipped tubes resulting from different modifications share the same structure. Flipped tubes are, however, the largest diameter DNA tubes thus far observed and thus are worthy of further characterization.

The ability to chemically differentiate the interior and exterior of DNA nanotubes, as demonstrated here, together with the ability to select molecules that enter the nanotubes based on size, as partially developed here, may have several uses. DNA nanotubes with catalysts inside might be used as size-specific reaction vessels. Further, because the inside of different DNA nanotubes are isolated from each other, chemical reactions that need to remain separate might be performed in the same sample. Such experiments would demonstrate compartmentalization, a theme essential to the organization of biological cells.

The programmability of DNA tile sets may allow us (1) to answer questions about DNA nanotubes that would otherwise be difficult and (2) to tune the physical properties of the nanotubes. For example, the dependence of persistence length and the kinetics of tube assembly on tube diameter currently cannot be measured because of tube polydispersity. This could be addressed with the creation of a series of defined-size tubes. A simple approach would use the progammability of tile sets to select a specific circumference from the natural variation. Diagonally striped REd+SEd tubes are constrained to have an even number of tiles in cross-section. In general, a diagonally striped tile set with N distinct tile types would force the circumference to be a multiple of N. For N at the upper range of the natural variation, say N = 10, we would expect only a single size of tube to form. In addition to providing defined-size tubes for study, this strategy may decrease defect rates and allow the selective preparation of large diameter tubes; either effect might yield tubes with persistence length significantly beyond the ∼4 μm length observed here. Also exciting is the possibility that computations may be embedded in the self-assembly of tubes, as has been done for lattices.[26] A binary counter[40] might be used to create tubes of programmable length.

In conclusion, our results show that DNA-only nanotubes can be designed to self-assemble based on simple geometrical principles that respect Watson−Crick base pairing, helix stacking at sticky ends, and the geometry of the major and minor grooves. Further, the formation of tubes is robust to a variety of changes. Reprogramming of the tile sets to create different patterns or the addition of decorations such as hairpins on the outside of the tubes shows little effect. However, modifications of the tiles that locate bulky hairpin groups in the interior or interstices of the tube, that disrupt stacking at the sticky-end contacts, or that change the intertile helix by more than one base pair all prevent normal tube growth, in agreement with the model. Thus, we believe that the DNA nanotubes described here, together with their design principles and the understanding gained in their characterization, will find significant use in DNA nanotechnology.

Acknowledgment. For useful discussions we thank Matthew Cook and Hideo Mabuchi. We thank the Caltech Molecular

(36) Bustamante, C.; Marko, J. F.; Siggia, E. D.; Smith, S. *Science* **1994**, *265*(5178), 1599−1600.
(37) Janmey, P. A.; Hvidt, S.; Kas, J.; Lerche, D.; Maggs, A.; Sackmann, E.; Schliwa, M.; Stossel, T. P. *J. Biol. Chem.* **1994**, *269*, 32503−32513.
(38) Krishnan, A.; Dujardin, E.; Ebbesen, T. W.; Yianilos, P. N.; Treacy, M. M. J. *Phys. Rev. B: Condens. Matter* **1998**, *58*, 14013−14019.
(39) Gittes, F.; Mickey, B.; Nettleton, J.; Howard, J. *J. Cell Biol.* **1993**, *12*, 923−934.
(40) Rothemund, P. W. K.; Winfree, E. In *Symposium on Theory of Computing (STOC)*; Association for Computing Machinery: New York, 2000.

Materials Research Center for use of their AFM scanners. P.W.K.R. was supported by a Beckman Fellowship. This work was supported in part by National Science Foundation CAREER Grant No. 0093486 and MRSEC Award DMR00-80034, DARPA BioComputation Contract F30602-01-2-0561, NASA NRA2-37143, an Army Research Office/UCSB Institute for Collaborative Biotechnologies Grant, an Alfred P. Sloan Foundation Fellowship (D.K.F.), and a grant from GenTel Corporation.

Supporting Information Available: Experimental methods, a discussion of the effect of hairpins on tube adhesion to mica, the derivation of the persistence length, and a discussion of the effect of hairpins, sticky-end stacking, and arm length on tube morphology; diagrams of lattice symmetries, a graph of the strain predicted for lattices of different symmetries, diagrams for the DX molecules used, sequences for all DNA strands, AFM and light micrographs of interesting tubes not in the text, graphs and fits for the peristence length data, gel-electrophoresis data for streptavidin binding studies, and a table summarizing the morphology and diameter of all observed variations of the tubes; two AFM movies of tubes opening, as well as a third movie showing a rotating view of the tube model. This information is available free of charge via the Internet at http://pubs.acs.org.

JA044319L